IEEE Access
Multidisciplinary ⋮ Rapid Review ⋮ Open Access Journal

Received January 13, 2022, accepted January 29, 2022, date of publication February 4, 2022, date of current version February 10, 2022.

*Digital Object Identifier 10.1109/ACCESS.2022.3149103*

# Online Detection of Out-of-Step Condition Using PMU-Determined System Impedances

**MARKO TEALANE[1], (Student Member, IEEE), JAKO KILTER[1], (Senior Member, IEEE), MARJAN POPOV[2], (Fellow, IEEE), OLEG BAGLEYBTER[3], AND DANNY KLAAR[4]**

[1]Department of Electrical Power Engineering and Mechatronics, Tallinn University of Technology, 19086 Tallinn, Estonia
[2]Faculty of EEMCS, Delft University of Technology, 2628 Delft, The Netherlands
[3]Grid Automation, GE Renewable, Edinburgh EH10 4QE, U.K.
[4]TenneT TSO B.V., 6812 Arnhem, The Netherlands

Corresponding author: Marjan Popov (m.popov@tudelft.nl)

This work was supported in part by the SA Archimedes Foundation Kristjan Jaak Scholarship under Grant 16-3.5/1470; in part by the Esi-Bida and ReSident Project by the Dutch Scientific Council De Nederlandse Organisatie voor Wetenschappelijk Onderzoek (NWO) under Grant 647.003.004; and in part by the Project and the Consortium Consisting of Transmission System Operator (TSO) TenneT, Distribution System Operators (DSOs) Alliander-Qirion, Stedin, Enduris, and General Electric and VSL.

**ABSTRACT** This paper presents a robust and adaptive out-of-step (OOS) protection algorithm, using wide-area information, that can be applied on tie-lines in observable power systems. The developed algorithm is based upon real-time computation of the system impedance and makes use of the well-known power-angle characteristic. In this way, a setting-less OOS concept in real-time environment is developed, which is applicable for tie-lines in an arbitrary power system. Furthermore, the developed protection algorithm is installed on hardware and is verified by numerous tests. The performance of the new hardware implementation is compared to the traditional impedance-based OOS protection methods. The results confirm that the proposed algorithm detects OOS conditions faster and more reliably than the traditional impedance-based solutions.

**INDEX TERMS** Out-of-step protection, power system transient stability, tie-lines, real-time HiL testing.

## I. INTRODUCTION

Severe faults can cause large deviations of electric power supplied by the generators in electric power systems. Generator prime movers are unable to quickly react to these changes, thus the imbalance between mechanical and electric power causes generator rotor speed variations, which result in power flow fluctuations in the network. Depending on the severity of these disturbances and the applied controls, the generators can either reach a new stable equilibrium point (through the process known as a stable power swing) or lose synchronism with each other and run in an out-of-step (OOS) condition.

This OOS condition should be identified and reacted to as quickly as possible in order to limit the amount of stress on the power system components. For this purpose dedicated OOS detection relays are installed in the power grids. These are usually installed on generators and transmission tie-lines, depending on power grid topology and system dynamics. Commercially, the most widely used method for detecting OOS conditions is based on the impedance measurement trajectory in order to distinguish between short circuit faults, recoverable power swings and OOS conditions [1], [2]. By adopting impedance-based method, the minimum measured impedance during the swinging period can be used to determine the electrical swing centre during oscillations. This approach, however, is sensitive to network reconfiguration as well as to load or generation changes, as predetermined settings are needed. These settings should be calculated offline, and because their determination requires extensive system studies, they cannot account for real-time changes in the network. Several other OOS detection methods are also proposed in the literature.

Table 1 presents a brief review of existing approaches in the industry and proposed methods in the literature to consistently detect an OOS condition. The advantages and certain limitations of the methods are also highlighted.

Additionally to the methods listed in the comparative table, some recent work on OOS protection based on local, bay level, measurements include [18], [19] and [20]. These methods, however, can only be applied on generator terminals, since they require direct input from generator measurements.

The associate editor coordinating the review of this manuscript and approving it for publication was Sarasij Das.

**TABLE 1. Existing OOS protection methods and approaches in literature and industry.**

| Classification | Method | Advantages | Limitations |
|---|---|---|---|
| Commercially available OOS detection approaches | Impedance based detection [1] [2] | Depending on the implementation, possess ability to differentiate stable and unstable swings | Difficulties in detecting very fast swings, rigorous analysis is required for setting the blinders. |
| | Angle-controlled OOS protection [3] | More reliable and faster than impedance-based OOS protection | Needs predetermined settings to operate and cannot adapt to system reconfigurations. |
| | R-Rdot method [4] | Faster detection than impedance based detection | Requires more computing capacity than the impedance based method. |
| | Superimposed current detection [5] | Very fast swing detection, ability to detect very fast swings. | Difficulties in detecting very slow swings, no differentiation between a stable and unstable swing |
| Unconventional OOS detection approaches based on local measurements | Power-time ($P$-$t$) curve based detection [6] [7] | Instability is directly detected from measurements | Can only be applied directly at generator terminals. Not yet implemented in a prototype. |
| | Faster than real-time OOS detection [8] | Provides extremely fast OOS detection. | Requires very detailed knowledge about generator parameters, can only be applied directly at generator terminals. |
| | Lyapunov function based OOS detection [9] | Method shows excellent results in OOS detection | Not yet implemented in a prototype. |
| Unconventional OOS detection based on wide-area information | Direct angle difference measurement based OOS protection [10] | Method does not require any computation of protection settings. | Requires monitoring of all the generator buses in the network. |
| | Predictive OOS based on synchrophasors [11] | Enhances existing OOS protection, provides more secure and reliable operation compared to existing methods. Has been proven in a prototype installation. | OOS detection speed is not known, is not effective in detecting non-oscillatory unstable swings. |
| | Swing center voltage estimation and analytic geometry parameters [12] | Provides settingless OOS protection, has been prototyped in a real industrial system. | OOS detection speed is not elaborated. |
| | Machine learning based approaches [13] [14] [15] | Methods offer fast and accurate OOS condition detection. | The correct performance of the methods require extensive training using detailed model. Not implemented in a prototype. |
| | **Proposed approach** | The method adapts to grid condition changes in real-time, is settingless and requires only two measurement location. Provides faster and more reliable OOS detection than conventional approaches, and has been prototyped. | Not yet implemented in a real network installation. |
| | Fast online coherency OOS detecion [16] | The method shows more reliable OOS detection than conventional solutions. | OOS detection speed is not elaborated, not yet implemented in a prototype |
| | Voltage fluctuations based OOS detection [17] | The method shows fast detection of instability. | Not yet implemented in a prototype |

An adaptive OOS relay design and application based on wide-area measurements utilising an equal-area criterion had already been proposed more than 20 years ago [21]. This approach relies on checking the measurement data against pre-stored network, generation and load data as well as breaker and line data and requires complex offline studies to function. In more recent years, a number of effective methods have been developed for detection of OOS conditions based on wide-area information - some of the most notable work includes [22]–[24] and [25]. All these methods, however, rely on measurements that are located directly at all of the generator terminals, or at the corresponding high-voltage terminals. This limiting factor is often overlooked and therefore makes the developed methods difficult to apply in real power systems due to the lack of coverage of PMUs in a large power system.

This paper proposes a novel approach for OOS detection and tripping based on computing the approximate angle difference between the centres of inertia on either end of a tie-line, thus relying only on two measurement locations in

a wide-area measurement system. The new method makes use of the computed system impedances at the remote ends of the tie-lines, where the algorithm is applied, to represent the whole network behind both ends of the tie-line as a two-machine equivalent system. A theoretical Last Stable Angle (*LSA*) value is found from the previously computed equivalent machine angles, which changes according to loading and grid conditions. After a disturbance takes place, the angle and its change between two equivalent sources is computed and compared to the *LSA* value.

The proposed algorithm is developed and verified in two stages - firstly by using software-in-the-loop simulations and thereafter by using real-time digital simulator to stream PMU data of a test network to a commercially available PhasorController device utilizing hardware-in-the-loop testing. The performance of the hardware implementation of the developed algorithm is firstly compared to the software implementation, and thereafter case studies for performance evaluation are performed in conjunction with two commercially available impedance-based out-of-step protection relays. The case studies performed show, that the developed algorithm operates faster and is more reliable in detecting out-of-step conditions compared to current out-of-step protection solutions.

The rest of the paper is organised as follows: Section II presents the proposed algorithm; Section III describes the methodology for testing the algorithm; Section IV shows case studies performed along with the results, and, finally, the paper ends up with meaningful conclusions being drawn.

## II. PROPOSED ALGORITHM

### A. EQUIVALENT SYSTEM

The idea behind the developed algorithm is that the bulk system can be simplified by using the assumption made in [26]; a multi-machine system can be separated into two groups around a tie-line. The simplified two-machine - system constructed around the observed tie-line can be reduced to a single machine infinite bus (SMIB) equivalent system with the parameters $\delta$, $\omega_s$, $M$, $P_m$ and $P_e$. The reduction process is described in detail in [26]. With the classical representation, the generator dynamics can be represented by the swing equation (1),

$$\frac{M}{\omega_s}\frac{d^2\delta}{dt^2} = P_m - P_e(\delta) \tag{1}$$

where $M$ - inertia constant of the equivalent machine; $\omega_s$ - rotor speed of the generator; $\delta$ - internal voltage angle of the generator; $P_m$ - mechanical input power of the generator; $P_e$ - electrical output power of the generator.

The electrical output power of the generator depends on the angle difference between the receiving system voltage phasor and the generator internal voltage phasor, the magnitudes of voltage phasors and the total system impedance between generator and the system. The generator's electrical output power can be represented by equation (2),

$$P_e(\delta) = \frac{|E_1||E_2|}{x_{tot}} sin\delta \tag{2}$$

where $|E_1|$, $|E_2|$ - are the equivalent internal voltage magnitudes of the machines; $x_{tot}$ - is total reactance between the two sources, and $\delta$ - is angle difference of the equivalent phasors.

By using the power-angle curve, the generator stability can be determined. The stability is directly linked to the internal angle differences of the two equivalent sources. On the power-angle characteristic, two operating points can be fixed by generator preloading and the electrical power curve as shown in Fig. 1a. The operating point located in the first half of the characteristic is a stable operating point. According to the Equal Area Criterion, the maximum angle difference for a recoverable swing cannot be greater than the second operating point, though it may be smaller. Further increase of the angle difference beyond *LSA* will definitively result in an unstable generator operation. Therefore, the *LSA* point is critical to distinguish between a stable and unstable swing. In order to assess this *LSA* point, the impedances of the equivalent sources must be known.

### B. EQUIVALENT SYSTEM IMPEDANCE COMPUTATION

The concept of the determination of the system's actual strength or the Thevenin impedance of a power network based on local measurements and small disturbances (such as load changes) was explored in [27]. This method describes the estimation of short-circuit impedance for a particular node in a power system. The Thevenin equivalent of the system $\underline{Z}_{eq}$, which is seen at the monitored location, is calculated from the recorded PMU voltage and current measurements. The scheme of impedance computation is illustrated in Fig. 1b, where the measured voltage and current phasors at the bus are denoted by $\underline{V}$ and $\underline{I}$.

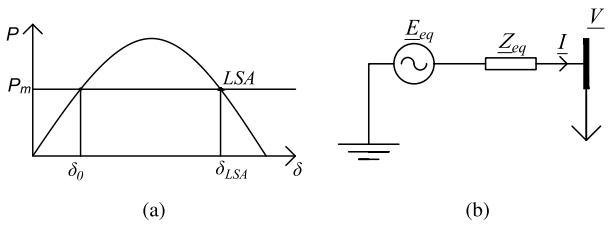


**FIGURE 1. (a) Power-angle curve constructed from calculated values, with Last Stable angle point denoted as *LSA*. (b) Equivalent impedance computation scheme illustration.**

In order to find the upstream system impedance from the locally measured quantities, two assumptions should be taken into account: 1) the downstream load is volatile; 2) during this variation the system remains constant. Voltage $\underline{V}(t)$ and current $\underline{I}(t)$ are measured and sampled at instants $t_1$ and $t_2$, which correspond to the pre-and post-disturbance values in the measured signals. Hence, the equivalent impedance

$\underline{Z}_{eq}$ can be found by using the following equation [27]:

$$\underline{Z}_{eq} = -\frac{\underline{V}(t_2) - \underline{V}(t_1)}{\underline{I}(t_2) - \underline{I}(t_1)} = -\frac{\Delta \underline{V}}{\Delta \underline{I}} \tag{3}$$

The delta value limits to compute the system impedance can be set empirically [27]. Alternatively, in order to improve the accuracy and the noise reduction of the measurements, an adaptive threshold can be used, as proposed in [28]. In this paper, the threshold values for detecting a disturbance are set empirically to 1 % of the primary measurement quantity, so that the impedance computation is not triggered by the ambient noise in the measurements. In addition, the impedance computation is vulnerable to phasor drift due to off-nominal system frequency, in which these can shift the angle during the time pre- and post-disturbance quantity sampling takes place. This problem, however, can be overcome by compensating the phasor drift as suggested in [29]. The sampling of voltage and current components is shown in Fig. 2b and Fig. 2a respectively, which, after sampling, are used to compute $\underline{Z}_{eq}$ according to Eq. (5).

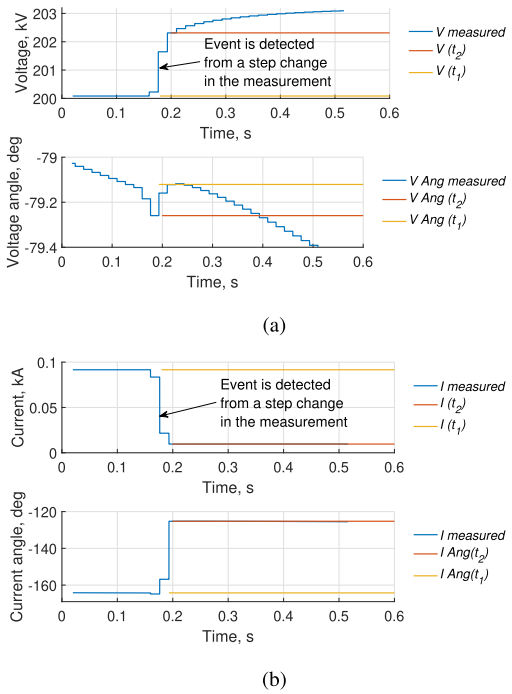


**FIGURE 2.** Voltage magnitude and angle sampling (a) and current magnitude and angle sampling (b) in the case of a step change. The pre-disturbance samples are denoted by $t_1$ and post-disturbance values by $t_2$.

It can be concluded that the computation of system impedance is only directly applicable in the case of a radial network, since in a meshed network all sources contribute to the actual changes in currents and voltages. Therefore, the total change in current and voltage behind the measured tie-line cannot be observed from one location. The same concept, however, can still be used to determine the system equivalent by making use of the superposition criterion, and utilising two measurement points.

Hence, for the system impedance computation of meshed networks, this method requires current measurement at two feeders in the same substation. An illustration of this is shown in Fig. 3, where one PMU measures bus voltage ($\underline{V}_1$), the currents of the tie-line ($\underline{I}_{tl}$) and, additionally, a load feeder ($\underline{I}_{r1}$), in which a step change in load may occur. In the figure a step change in a load feeder is caused by a reactor, although a capacitor bank, a filter or other volatile load could be used. A second PMU measures the same feeders and parameters at the other end of the tie-line.

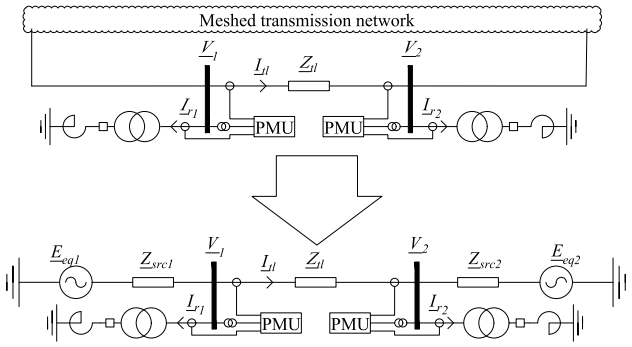


**FIGURE 3.** Principle scheme for system impedance estimation on meshed networks.

Whenever a step change in the measured current or voltage occurs, e.g. due to switching of the reactor in the load feeder, the system impedance is determined according to (3). Hence, by applying the superposition criterion, the system equivalent impedance $\underline{Z}_{src1}$ behind the measured tie-line at bus 1 in Fig. 3 can be calculated using the proportional change of current in the measured load feeder and the change of the tie-line current as follows:

The approach proposed in (4) is used as a basis to compute the system impedance behind the tie-line, which is needed to determine the LSA threshold. Protection operation and OOS condition identification are based on that determined concept.

$$\begin{aligned}\underline{Z}_{src1} &= -\frac{\underline{V}_1(t_2) - \underline{V}_1(t_1)}{\underline{I}_{r1}(t_2) - \underline{I}_{r1}(t_1)} \\ &\quad \cdot \frac{(\underline{I}_{r1}(t_1) - \underline{I}_{r1}(t_2))}{(\underline{I}_{r1}(t_1) - \underline{I}_{r1}(t_2)) - (\underline{I}_{tl}(t_1) - \underline{I}_{tl}(t_2))} \\ &= -\frac{\Delta \underline{V}_1}{\Delta \underline{I}_{r1}} \frac{\Delta \underline{I}_{r1}}{\Delta \underline{I}_{r1} - \Delta \underline{I}_{tl}} = -\frac{\Delta \underline{V}_1}{\Delta \underline{I}_{r1} - \Delta \underline{I}_{tl}}\end{aligned} \tag{4}$$

### C. DEVELOPING OUT-OF-STEP PROTECTION CONCEPT

The proposed OOS protection solution is based on the change of computed voltage phasors of the two equivalent sources behind the computed impedances located at the remote ends of the observed tie-lines. The required equivalent system voltage is accordingly computed at both ends of the tie-line as follows:

$$\begin{aligned}\underline{E}_{eq1} &= \underline{Z}_{eq1} \cdot \underline{I}_{tl} + \underline{V}_1 \\ \underline{E}_{eq2} &= \underline{Z}_{eq2} \cdot \underline{I}_{tl} + \underline{V}_2\end{aligned} \tag{5}$$

For the equivalent system depicted in Fig. 3, the angle difference between the two equivalent generator voltages is illustrated in Fig. 4.

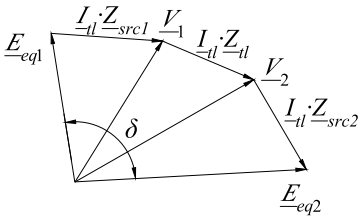


**FIGURE 4.** Equivalent phasor diagram constructed from computed equivalent system impedances and measured quantities.

In this way, from the angle difference the power-angle curve is then determined, and the *LSA* point (noted as $\delta_{LSA}$ on Fig. 1) is computed. The *LSA* point is fixed by using the angle difference of the equivalent vectors as $\pi - \delta_0$. This value is continuously recalculated by using the measurement values and the previously obtained equivalent impedances.

During an OOS condition, the angle difference between the two equivalent source voltages increases over the *LSA* point. The protection will declare an OOS condition when the following conditions are met:

$$\begin{cases} \delta > \delta_{LSA} & \text{for two consecutive measurements} \\ \dfrac{d\delta}{dt} > 0 & \text{for two consecutive measurements} \\ V_1 > 0.5p.u. & \\ V_2 > 0.5p.u. & \\ \dfrac{d\delta}{dt} < 20\pi \dfrac{rad}{s} & \text{for two consecutive measurements} \end{cases}$$

The first two criteria indicate that the angle difference exceeded the LSA and is continuing to increase. The last three criteria, are used as a safety feature to block the protection from maloperation when a short-circuit fault occurs.

Voltage thresholds with the value of 0.5 p.u. have been set to verify whether the tie-line is energised and no fault is present on the line. The $\frac{d\delta}{dt}$ threshold acts as an additional fault-detection mechanism, and prevents the protection operation due to oscillations with high frequency. During a fault occurrence there will be a high step change of the computed angle value, which might exceed the *LSA* for the duration of the fault. Nevertheless, the protection must not operate during a fault. A derivative setting value of $20\pi \frac{rad}{s}$, in this case with a 60 Hz power system, enables the protection to detect power system oscillations with the frequency of up to 10 Hz. These blocking criteria can be adjusted freely if more protection sensitivity or security are required. When any of the blocking criteria of the protection are fulfilled, the OOS algorithm operation will be blocked for 200 ms. If thereafter any of the criteria are still fulfilled, the blocking will be applied until the drop-off of the criterion.

The *LSA* point is limited to a minimum of 90 degrees, in order to avoid it being set in the first half of the power-angle characteristic. At the same time, the *LSA* point is limited to a maximum of 130 degrees. This is important, because the protection should be still operational during low or no load current in the observed tie-line before the *LSA* value is sampled.

### D. HARDWARE IMPLEMENTATION OF THE DEVELOPED ALGORITHM

In order to compare the developed algorithm's performance to already existing commercial solutions, it was adapted and installed on external hardware using a commercially available PhasorController (PhC) [30]. The algorithm is divided into four main partfs and the structure of the implemented algorithm on hardware was organised as shown in Fig. 5.

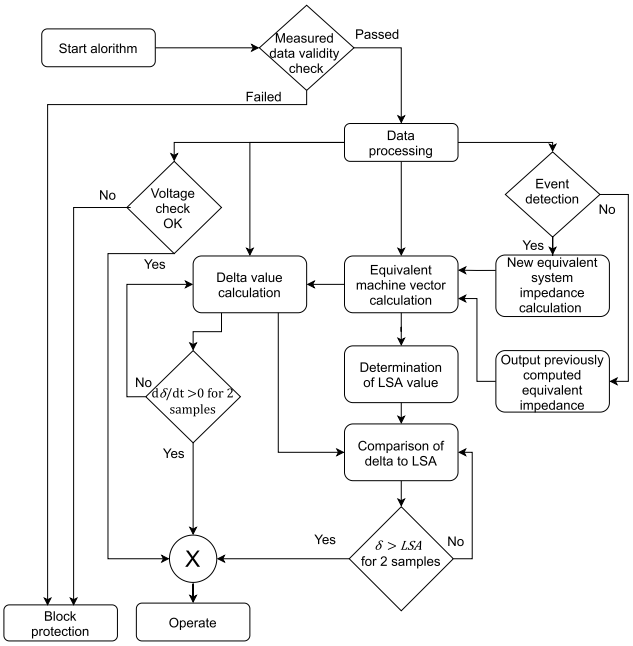


**FIGURE 5.** Principle diagram of the developed algorithm in industrial controller.

Valid PMU measurement signals must be collected from both measurement points in the network in order for the algorithm to operate. The data validity is checked and handled by the PhC, and the check is performed before the data is going to be processed. If the measured data does not pass the validity check, meaning the data is not time synchronized or is missing, then the protection algorithm is blocked. When the validity check is passed, then the voltage values of the measurement points are checked and compared to the threshold values in order to detect short-circuit faults. If any measurement point has a lower voltage value than the specified threshold, the protection is blocked for the predetermined time, until the voltage has been restored in the network. This is done in order to avoid maloperations during short-circuit faults in the network, when the PMU measurements are affected by fault conditions and do not represent the electromechanical behavior of the grid.

At the same time, the data measurements provide input to the event detection for impedance calculation. Upon detecting a step change in the measurement quantities, the event detection block stores the measured values, which are then used to compute the equivalent impedance needed for the equivalent voltage vector computation as shown in (2). When no event is detected in the measurement data, the event detection block will output the previously computed equivalent impedance values to the vector computation.

By utilizing the measured voltage vectors and currents, the equivalent machine vectors of the centres of inertia are computed according to (5). Using the computed equivalent machine vectors, the *LSA* value is fixed every time a new equivalent impedance value is provided. The *LSA* value is computed using the difference in angular value of the two computed equivalent machine vectors according to power-angle characteristic as $\pi - \delta$. In parallel, the current $\delta$ value is being computed continuously and compared against the determined threshold value. When the $\delta$ value exceeds the determined *LSA* value for more than two samples, and the derivative of $\delta$ has been positive for the past two samples, the protection sends a trip command.

## III. TESTING METHODOLOGY AND TEST SETUP

The performance of the algorithm is investigated by applying it in the IEEE 39 bus network model. The network is modified by adding generic grid-following wind farms (W1 - W5) at some buses. The model used for the power plants is described in [31]. In this way, the developed solution can be tested for different grid conditions. The modified test network is shown in Fig. 6. Two different test locations are chosen to show the developed solution's suitability for arbitrarily chosen tie-lines. The first test location is circled in red and shown as Case A, and the other is circled in blue and is denoted as Case B. Case A is an example to observe power swings between two areas, whilst Case B demonstrates power swings in a single machine system connected to an infinite bus system.

For both locations, two tie-lines were observed in order to see the proposed algorithm's behaviour for various grid conditions. For Case A, the protection was tested for the lines between buses 14-15 and 16-17. To create an OOS condition, a three phase short circuit is made on bus 16. The fault is cleared by disconnecting one of the transmission lines emanating from bus 16. For Case B, the transmission lines under observation are between buses 26-29 and 28-29. Power swings are created by a three-phase short circuit applied on bus 29. The fault is cleared by disconnecting one of the two tie-lines connected to this bus. This contingency causes power swings along the remaining transmission lines.

In addition, the proposed algorithm is installed on a PhC and tested in parallel with two physical relays. Both relays incorporate an impedance based OOS algorithm and are set up to trip on the way in (TOWI) and trip on the way out (TOWO) of the configured impedance characteristic. The settings of the protection devices are obtained according to

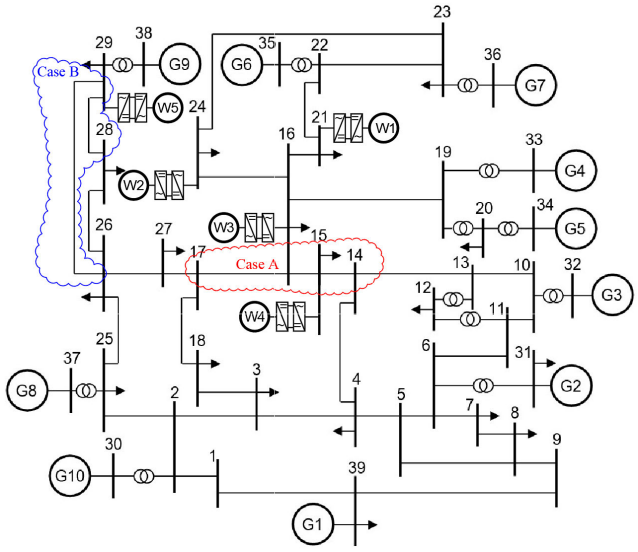


**FIGURE 6.** Modified IEEE 39 bus network with added type 4 wind farms. Red marks Case A testing location and blue Case B testing location, wind farms are added to buses 21, 15, 25, 16 and 29.

the manufacturer's guidelines as explained in the user manuals of the relays'; the settings are calculated by using a base case of fully synchronous system [32], [33]. The protective relays, together with the PhC, are tested by applying hardware-in-the-loop (HiL) tests, and the results obtained are compared to the applied concept described in Section II. An illustration of the experimental setup is provided in Fig. 7. The PhC device, where the proposed algorithm is implemented, receives measurement data over the network according to IEEE C37.118 standard. Different data rates would have an effect on the decision time of the algorithm, since the algorithm's criteria are linked to consecutive measurements. Therefore, the slower the data date, the slower the decision time. For uniformity throughout the paper, the data rate used for PMU data for all the conducted tests is 60 Hz. The PhC provides feedback about operation and measured values back to the Real-Time Digital Simulator using IEC61850 GOOSE messages. The protection relays, situated on lines 16-17, 15-14, and at the line remote ends near bus 29 for cases A and B respectively, receive analogue signals through signal amplifiers connected to the simulator. Protection relay output signals are provided as digital input signals to the simulator.

In order to test the protections for various grid conditions, the output power of the windfarms is scaled up while simultaneously decreasing the synchronous generation capacity. In Case A, for a specific renewable energy penetration scenario (RES %), all four windfarms (denoted as W1 - W4 on Fig. 6) in the network area provide the specific percentage of the base case synchronous generation output of the four generators (denoted as G4, G5, G6 and G7) in the area. At the same time, the apparent power of these generators is decreased from the initial value of 1000 MVA by the same specific percentage of the RES % level. This is not only to

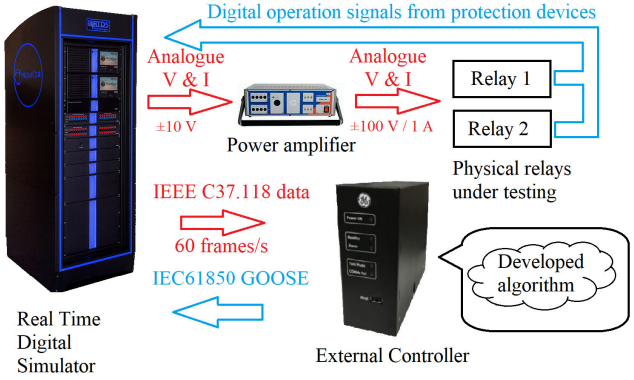


**FIGURE 7.** Experimental setup for OOS protection testing using physical hardware.

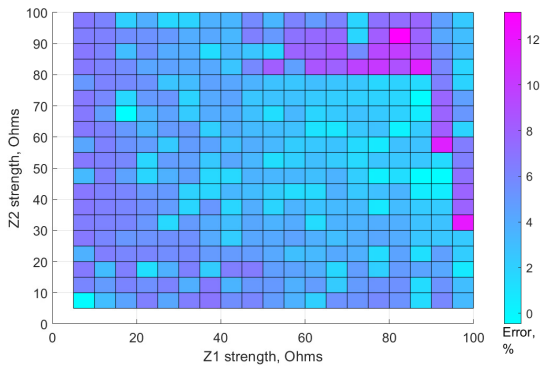


**FIGURE 9.** Absolute error in the impedance computation on Side 2 of the test network related to the system impedances.

decrease the output of the generation, but also to decrease the system inertia. For Case B, the scaling is performed for one generator (G9) and one windfarm (W5). Besides this, each test case is repeated five times to verify that the algorithm detects OOS conditions.

## IV. CASE STUDIES

### A. IMPEDANCE COMPUTATION

For testing and verifying the impedance computation part of the developed algorithm, a simple system with variable system impedances on either side of the transmission line, as shown in Fig. 8, was built. One of the impedance buses is chosen to be close to the source, representing a generator bus, whilst the other is located in the middle of the system to represent an arbitrary node in a system. The test system nominal voltage is 345 kV and with a frequency of 60 Hz. To test the accuracy of the system impedance computation, the two system impedances are varied between 5 Ohm and 100 Ohm.

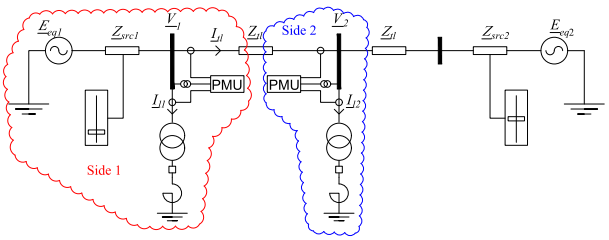


**FIGURE 8.** Test network for testing impedance computation of the developed algorithm.

In this work, the RTDS library models of the PMUs are used [34]. For side 1 in red in Fig. 8, the average absolute impedance computation error is 0.3% with a standard deviation of 0.55%. Therefore, this impedance computation is considered reliable. For side 2, the average absolute impedance computation error is 4.2% with a standard deviation of 2.15%. The error of the computed impedance depends on system impedances and is shown in Fig. 9. It can be noted this error increases when the system impedance increases. The impedance behind the measurement point on Side 2 has a greater influence on the system impedance computation. The maximum error of the impedance computation is computed as 13.2%.

### B. TESTING RESULTS FOR THE DEVELOPED ALGORITHM

The lab environment network latency from the RTDS to the industrial controller was measured to be under 1 ms. However, in order to represent a more realistic scenario, a Phasor Data Concentrator (PDC) Wait Time setting of 100 ms was implemented in the PhC, which is representative of real-world PMU applications. Normally, the PDC Wait Time setting means that in order to align the measurement data from different PMUs in the network, the controller will wait for a period of time until the measurements arrive. Thereafter, the processing of the measurements will begin in the logic built inside the device.

In order to verify the security of the developed algorithm, the $\delta$ value and generators' reaction for a five-cycle fault on bus 16, followed by the disconnection of line between bus 16 and 17, is shown in Fig. 10. The proposed OOS protection is demonstrated on a transmission line between buses 15 and 14. The upper figure shows the generator angle, and it can be seen that the fault produces a stable swing with stable generator angles. For the lower figure, the computed $\delta$ values of the RTDS and hardware implementations are shown. From the $\delta$ value plot, it can be observed that the value computed in the PhC is lagging behind the RTDS model application for around 110 ms. This is due to the applied PDC Wait Time setting and processing of the controller logic itself.

Fig. 11 shows the performance of the developed algorithm in RTDS and in the PhC for a six-cycle fault occurring on bus 16. This fault leads to an unstable swing causing generators 4 - 7 to go out-of-step with the rest of the system. This can clearly be seen in the upper figure, where the generator rotor angles are shown. In the lower figure, the computed $\delta$ values are shown for both RTDS and hardware implementation of the proposed algorithm. It is observed that due to the unstable swing in the network, the computed $\delta$ value exceeds the algorithm's predetermined *LSA* threshold and keeps increasing. This results in a trip command from the developed algorithm.

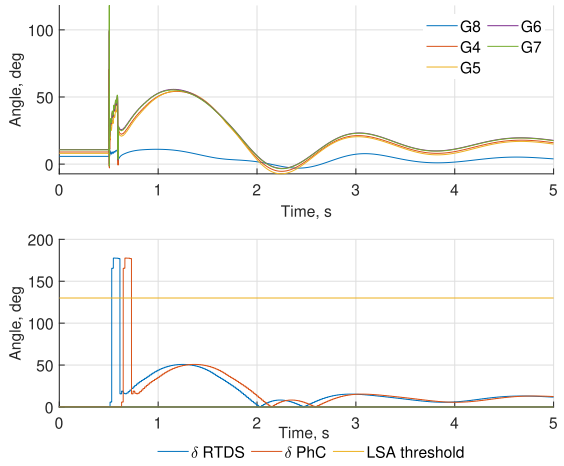


**FIGURE 10.** Generator angle response and $\delta$ value calculation response to a five-cycle long fault at bus 16.

The operation signals are represented by a green dashed line for RTDS implementation of the algorithm, and a magenta dashed line for the physical controller implementation. It can also be noted that the time shift of $\delta$ computation between the RTDS and hardware implementation of the algorithm is 110 ms.

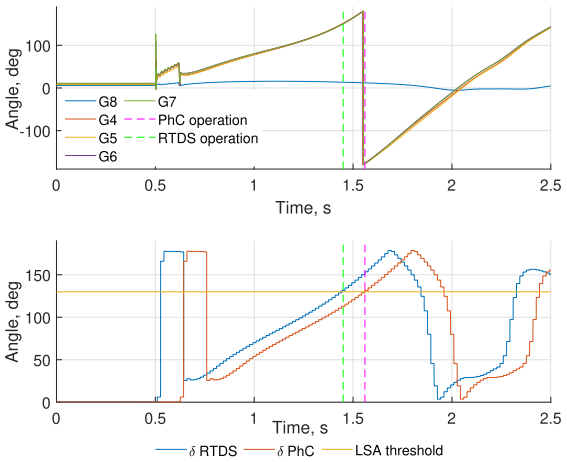


**FIGURE 11.** Generator angle response and $\delta$ value calculation response to a six-cycle long fault at bus 16.

OOS tripping speed and security can generally be evaluated by two criteria: a) the amount of time needed to report OOS condition after a fault is cleared, and b) the percentage of correct OOS detections. Comparisons of these two metrics between the RTDS and the hardware application of the proposed algorithm are shown in Fig. 12a and Fig. 12b respectively.

When looking at the average operation time in Fig. 12a, it can be seen that the hardware implementation shows higher operation times, than the RTDS implementation of the proposed algorithm. For Case A, the RTDS software implementation shows an average operation time of 1.14 s, whilst the controller implementation shows an average operation time of 1.32 s. This means that the controller shows an increase

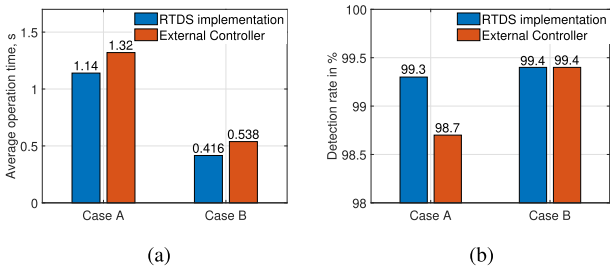


**FIGURE 12.** Comparisons of proposed algorithm performances: (a) Comparison of average operation times, (b) Comparison of percentage of OOS conditions detected.

of 180 ms in operating time. For Case B, the RTDS implementation shows an average operation time of 0.416 s, and the hardware implementation shows an average operating time of 0.538 s. Therefore the hardware implementation has, on average, 122 ms slower operating time for Case B. This is expected behavior due to the delays implemented in the PhC and logic processing of the developed algorithm in the controller.

In Fig. 12b, the detection rates of all of the OOS conditions for the performed tests of the algorithm are shown. It can be seen that there a 0.6% difference in the detection rates of RTDS and hardware implementation of the proposed algorithm for the performed tests in Case A. For Case B no difference in detection rates between the hardware and software implementation has been identified. Therefore, based on the performed analysis, it is safe to say that the hardware implementation of the proposed solution is successful and reliable.

### C. ALGORITHM RESPONSE FOR GRID EVENTS

The PhC implementation of the developed algorithm has been tested for various grid events. Two specific cases have been chosen and are explained in more detail. For this, the algorithm is installed on the IEEE 39 bus test system's line 14-15 and the algorithm's behavior for two faults is shown - a single-line to ground fault on the protected line and a two-phase fault outside of the protected line.

The algorithm's response for a single-line to ground fault on the protected line 14-15, and the subsequent one pole open condition, is shown in Fig. 13a. In the figure, the signals regarding the algorithm response is displayed on the first graph, and the second graph displays the computed $\delta$ value in the algorithm. The actual values during the event in the power system are shown in Fig. 13b, where the instantaneous current values from either end of the protected line can be seen on the first two graphs, and the last graph displays the generator rotor angle values. It can be seen from the instantaneous current values in the figure, that there is a single-phase fault on the transmission line, followed by a single-pole trip, which is thereafter reclosed after 0.4 seconds. From the protection reaction, it can be observed, that in both ends of the protected line the algorithm registers an event, however, following the event no blocking or operation signals are activated, therefore

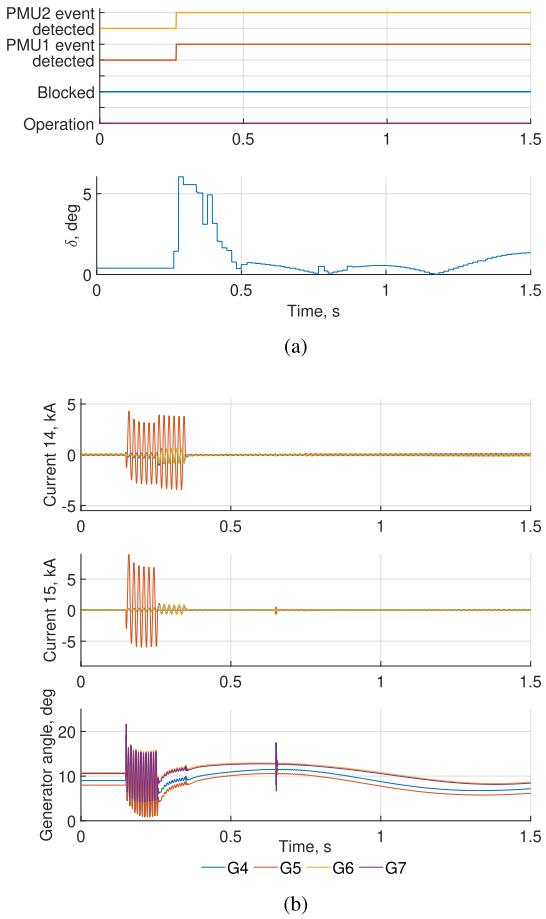


**FIGURE 13.** Algorithm resoponse and measurements in the case of a single-line to ground fault on the protected line. (a) shows the signals regarding the developed algorithm response and the computed $\delta$ value by the algorithm, (b) shows the instantaneous measurements from either end of the transmission line, where the protection has been installed, and the generator rotor angles in the system.

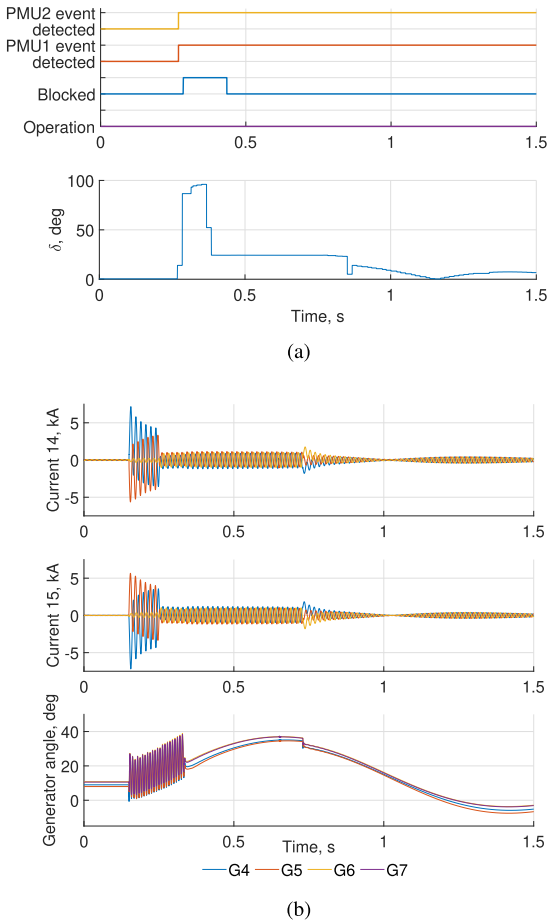


**FIGURE 14.** Algorithm resoponse and measurements in the case of an external two-phase fault. (a) shows the signals regarding the developed algorithm response and the computed $\delta$ value by the algorithm, (b) shows the instantaneous measurements from either end of the transmission line, where the protection has been installed, and the generator rotor angles in the system.

it can be concluded, that the developed algorithm shows stable operation during an internal single-phase fault, and during one pole open condition.

The algorithm's response to an external two-phase fault is shown in Fig. 14a. In this case, the protection is still installed on transmission line between buses 14-15, and the fault takes place on line 15-16, after which the faulted line is tripped and reclosed 0.4 seconds after tripping. In the figure, the signals related to the algorithm response is displayed on the first graph, and the second graph displays the computed $\delta$ value in the algorithm. The actual values during the event in the power system are shown in Fig. 14b, where the first two graphs show the instantaneous current values from either end of the protected line, and the last part of the graph displays the generator rotor angle values. Looking at the protection response, it can be seen, that, in a similar manner to a single-phase fault, event is picked up on both ends of the protected line. In this case, however, due to the fault type and location, the computed angular difference has a large jump, that causes the algorithm to be blocked from operation during a fault condition as explained in Section IIc. The computed angle value stabilizes to a constant value after the fault has been cleared, and the blocking of the protection function drops off. The algorithm does not issue an operation command, therefore it can be concluded, that the developed algorithm shows stable operation during external faults.

### *D. COMPARISON WITH IMPEDANCE PROTECTION FOR CASE A*

The test results of protection operation times for Case A are shown in Fig. 15a and Fig. 15b. The operation times shown in these figures are the times the protection needs to provide a trip command starting from the removal of the fault. The operation time of "0" means that the protection did not provide an OOS tripping command for a duration of five seconds after fault initiation; hence, the simulation was terminated without protection trip for all of the five conducted tests at that RES % scenario. Fig. 15a shows the operation times for a case study on tie-line between buses 14 and 15, which represents a longer line between the two system parts. It can be observed that when increasing RES penetration in one of the areas, the difference between the protection operations is narrowing.

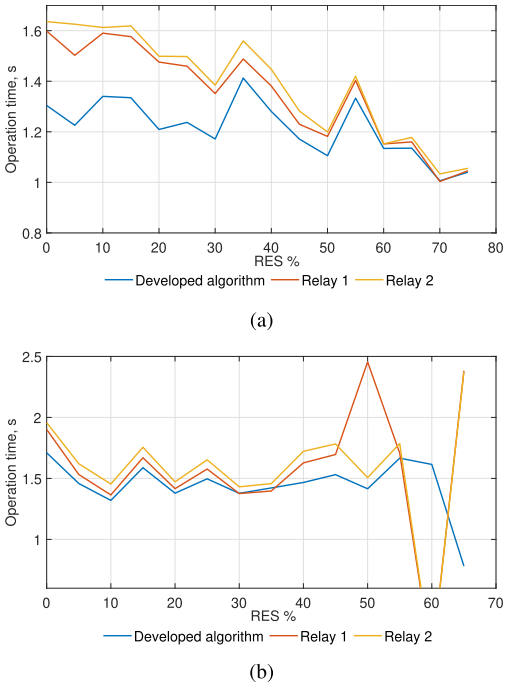


**FIGURE 15.** OOS tripping times of protection devices for Case A. (a) represents case study with a longer line (Line 14-15) between two systems and (b) represents a short line (Line 16-17) between two systems.

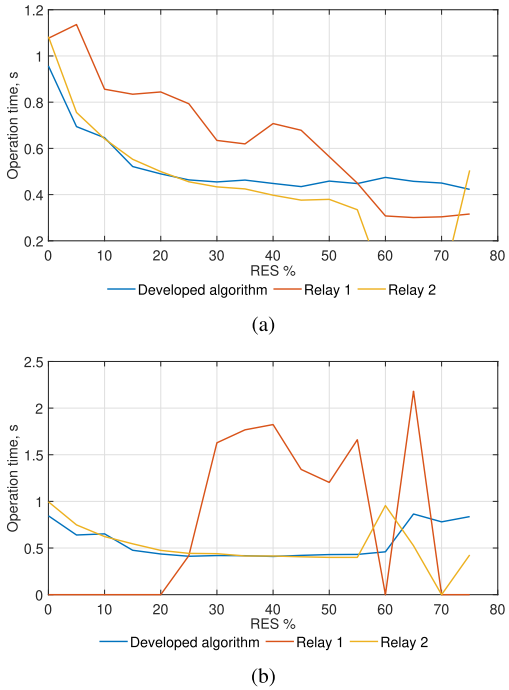


**FIGURE 16.** OOS tripping times of protection devices for Case B. (a) represents a long line (Line 26-29) between the machine and the system, (b) represents a short line (Line 28-29) between the machine and the system.

However, for all situations the developed algorithm in hardware implementation performs better, as faster OOS detection times are obtained than from the traditional impedance based protection.

For the shorter line testing results, as shown in Fig. 15b, the new method has faster OOS detection times than the traditional protections for almost all of the observed RES % scenarios. It can also be seen that the tested impedance based relays do not operate at all for RES penetration levels from 55% to 60%. For 65% RES penetration both relays operated only on the second unstable swing, which resulted in the significantly delayed operation.

### E. COMPARISON WITH IMPEDANCE PROTECTION FOR CASE B

The combined protection operations for both tested lines for Case B (SMIB) are shown in Fig. 16a and in Fig. 16b. Fig. 16a shows the results of the protection operating times versus the renewable energy penetration when an OOS condition was created on a longer tie-line. The blue line shows the operation times of the developed algorithm's hardware implementation, whilst the red and yellow lines show the operation times of physical relays. From this figure, it can be seen that the developed solution and Relay 2 have very similar operating times whilst Relay 1 operates around 200 ms slower. It can also be observed that Relay 2 does not detect the OOS condition between 65% and 75% of renewable penetration. In addition, starting from RES penetration of 60%, Relay 1 issues a tripping command not from OOS protection, but rather from the distance protection element, which results in a very short operation time. This is an obvious case of maloperation of the distance protection element, which may be caused by an incorrect configuration of the Power Swing Blocking element.

Fig. 16b shows the protection operating times versus RES % penetration for the case of OOS condition on the shorter tie-line. It can be seen that, as before, the developed solution and Relay 2 have very similar operating times for the tested renewable penetration levels, except for very high penetration scenarios. It should be noted that in this case Relay 1 (shown in red) scores the worst detection rate of the OOS condition, as it only operated consistently for RES penetration between 25 and 50%. The other physical relay did not experience similar difficulties in detecting an OOS condition; only failing to detect OOS at 75% RES penetration level.

## V. CONCLUSION

The paper introduces a novel robust and adaptive OOS protection algorithm for tie-lines based on PMU-determined system impedances. The algorithm successfully adapts to system condition changes by utilising on-line network impedance computation, and is based only upon two measurement points in the network. Hence, it is suitable to be applied on arbitrary tie-lines in every power system topology, where OOS conditions can occur. Case studies are carried out in SMIB, and IEEE39 bus test network, which demonstrate the effectiveness of the developed algorithm. A prototype of the algorithm is designed and validated in real-time using RTDS and an external industrial controller. For the HiL testing of the

prototype a PDC Waiting Time, or latency, of 100 ms has been used, to simulate real-world like conditions. The robustness and the efficiency of the developed algorithm are verified and compared against commercial OOS relays by conducting numerous tests for different network conditions including different penetration levels of renewable generation. The conducted research shows advantages over the existing methods, namely:

- For all studied cases, the proposed algorithm provides faster operation (up to 200 ms when implemented on actual hardware) compared to the existing impedance-based OOS methods which are currently used in commercially available relays.
- The proposed algorithm provides more reliable OOS detection than traditional impedance based solutions.
- The algorithm is very lightweight and needs little processing power, which offers possibility to be installed in already existing Phasor Data Concentrators or programmable logic devices.
- The algorithm does not require specific settings, therefore, no extensive offline studies of the power system are needed.

## REFERENCES


[1] D. A. Tziouvaras and D. Hou, "Out-of-step protection fundamentals and advancements," in *Proc. 57th Annu. Conf. Protective Relay Eng.*, 2004, pp. 282–307.

[2] J. Blumschein, Y. Yelgin, and M. Kereit, "Blackout prevention by power swing detection and out-of-step protection," *J. Power Energy Eng.*, vol. 2, no. 4, pp. 694–703, 2014.

[3] A. Sauhats, A. Utans, and E. Biela-Dalidovicha, "Equal area criterion and angle control-based out-of-step protection," in *Proc. IEEE 58th Int. Sci. Conf. Power Electr. Eng. Riga Tech. Univ. (RTUCON)*, Oct. 2017, pp. 1–6.

[4] C. W. Taylor, J. M. Haner, L. A. Hill, W. A. Mittelstadt, and R. L. Cresap, "A new out-of-step relay with rate of change of apparent resistance augmentation," *IEEE Trans. Power App. Syst.*, vol. PAS-102, no. 3, pp. 631–639, Mar. 1983.

[5] *MiCOM O40 Agile P543/P545 Technical manual Ver92M*, Schneider Electr., Rueil-Malmaison, France, 2021.

[6] S. Paudyal, R. Gokaraju, M. S. Sachdev, and S. Cheng, "Out-of-step detection using energy equilibrium criterion in time domain," *Electr. Power Compon. Syst.*, vol. 37, no. 7, pp. 714–739, Jun. 2009.

[7] S. Paudyal, G. Ramakrishna, and M. S. Sachdev, "Application of equal area criterion conditions in the time domain for out-of-step protection," *IEEE Trans. Power Del.*, vol. 25, no. 2, pp. 600–609, Apr. 2010.

[8] M. Abedini, M. Davarpanah, M. Sanaye-Pasand, S. M. Hashemi, and R. Iravani, "Generator out-of-step prediction based on faster-than-real-time analysis: Concepts and applications," *IEEE Trans. Power Syst.*, vol. 33, no. 4, pp. 4563–4573, Jul. 2018.

[9] K. Sreenivasachar, "Out-of-step detection on transmission lines using apparent impedance differential method," *IEEE Trans. Power Del.*, early access, Nov. 13, 2021, doi: 10.1109/TPWRD.2021.3125525.

[10] P. Regulski, W. Rebizant, M. Kereit, and H.-J. Herrmann, "PMU-based generator out-of-step protection," *IFAC-PapersOnLine*, vol. 51, no. 28, pp. 79–84, 2018.

[11] T. D. Duong, S. D'Arco, and A. Holdyk, "A method for predictive out-of-step tripping based on synchrophasors," in *Proc. 15th Int. Conf. Develop. Power Syst. Protection (DPSP)*, 2020, pp. 1–6.

[12] J. R. Camarillo-Penaranda, D. Celeita, M. Gutierrez, M. Toro, and G. Ramos, "An approach for out-of-step protection based on swing center voltage estimation and analytic geometry parameters," *IEEE Trans. Ind. Appl.*, vol. 56, no. 3, pp. 2402–2408, May 2020.

[13] N. G. Chothani, B. R. Bhalja, and U. B. Parikh, "New support vector machine-based digital relaying scheme for discrimination between power swing and fault," *IET Gener., Transmiss. Distrib.*, vol. 8, no. 1, pp. 17–25, Jan. 2014.

[14] M. R. Aghamohammadi and M. Abedi, "DT based intelligent predictor for out of step condition of generator by using PMU data," *Int. J. Electr. Power Energy Syst.*, vol. 99, pp. 95–106, Jul. 2018. [Online]. Available: https://www.sciencedirect.com/science/article/pii/S0142061517321397

[15] E. A. Frimpong, P. Y. Okyere, and J. Asumadu, "On-line determination of transient stability status using MLPNN," in *Proc. IEEE PES PowerAfrica*, Jun. 2017, pp. 23–27.

[16] D. Fan and V. Centeno, "Adaptive out-of-step protection schemes based on synchrophasors," in *Proc. IEEE PES Gen. Meeting|Conf. Exposit.*, Jul. 2014, pp. 1–5.

[17] K. Shimizu and A. Ishigame, "Novel transient stability assessment using post-disturbance voltage fluctuations," in *Proc. Int. Conf. Smart Grids Energy Syst. (SGES)*, Nov. 2020, pp. 12–17.

[18] M. R. Nasab and H. Yaghobi, "A real-time out-of-step protection strategy based on instantaneous active power deviation," *IEEE Trans. Power Del.*, vol. 36, no. 6, pp. 3590–3600, Dec. 2021.

[19] J. P. Desai and V. H. Makwana, "Phasor measurement unit incorporated adaptive out-of-step protection of synchronous generator," *J. Modern Power Syst. Clean Energy*, vol. 9, no. 5, pp. 1032–1042, 2021.

[20] B. Deshmukh, S. Biswal, and D. K. Lal, "Synchronous generator out-of-step protection based on Savitzky-Golay filtering technique," in *Proc. Emerg. Trends Ind. 4.0 (ETI 4.0)*, 2021, pp. 1–3.

[21] V. Centeno, A. G. Phadke, A. Edris, J. Benton, M. Gaudi, and G. Michel, "An adaptive out-of-step relay [for power system protection]," *IEEE Trans. Power Del.*, vol. 12, no. 1, pp. 61–71, Jan. 1997.

[22] Y. Cui, R. G. Kavasseri, and S. M. Brahma, "Dynamic state estimation assisted out-of-step detection for generators using angular difference," *IEEE Trans. Power Del.*, vol. 32, no. 3, pp. 1441–1449, Jun. 2017.

[23] J. R. A. K. Yellajosula, Y. Wei, M. Grebla, S. Paudyal, and B. A. Mork, "Online detection of power swing using approximate stability boundaries," *IEEE Trans. Power Del.*, vol. 35, no. 3, pp. 1220–1229, Jun. 2020.

[24] S. Zhang and Y. Zhang, "A novel out-of-step splitting protection based on the wide area information," *IEEE Trans. Smart Grid*, vol. 8, no. 1, pp. 41–51, Jan. 2017.

[25] H. Zare, H. Yaghobi, and Y. Alinejad-Beromi, "Adaptive concept of controlled islanding in power systems for wide-area out-of-step prediction of synchronous generators based on adaptive tripping index," *IET Gener., Transmiss. Distrib.*, vol. 12, no. 16, pp. 3829–3836, Sep. 2018.

[26] Y. Xue, T. Van Custem, and M. Ribbens-Pavella, "Extended equal area criterion justifications, generalizations, applications," *IEEE Trans. Power Syst.*, vol. 4, no. 1, pp. 44–52, Feb. 1989.

[27] K. O. H. Pedersen, A. H. Nielsen, and N. K. Poulsen, "Short-circuit impedance measurement," *IEE Proc.-Gener., Transmiss. Distrib.*, vol. 150, no. 2, pp. 169–174, Mar. 2003.

[28] Y. Wang, W. Xu, and J. Yong, "An adaptive threshold for robust system impedance estimation," *IEEE Trans. Power Syst.*, vol. 34, no. 5, pp. 3951–3953, Sep. 2019.

[29] B. Alinezhad and H. Kazemi Karegar, "On-line Thévenin impedance estimation based on PMU data and phase drift correction," *IEEE Trans. Smart Grid*, vol. 9, no. 2, pp. 1033–1042, Mar. 2018.

[30] GE Digital. (2021). *Phasor Controller*. [Online]. Available: https://www.ge.com/digital/applications/transmission/phasorcontroller

[31] *Modelling of Permanent Magnet Generator Based Wind Turbine Systems in the RTDS*, RTDS Technol., Winnipeg, MB, Canada, 2017.

[32] *SIPROTEC 4 Line Differential Protection with Distance Protection 7SD5 V4.7*, Siemens AG, Munich, Germany, 2016.

[33] *Easergy MiCOM P44y Technical Manual*, Schneider Electr., Rueil-Malmaison, France, 2019.

[34] *RSCAD Controls Libarary Manual*, RTDS Technol., Winnipeg, MB, Canada, 2021.


**MARKO TEALANE** (Student Member, IEEE) received the B.Sc. and M.Sc. degrees in electrical power engineering from the Tallinn University of Technology, in 2016 and 2018, respectively, where he is currently pursuing the Ph.D. degree in power engineering. He is currently a Researcher with the Tallinn University of Technology. His research interests include power system protection, power system relaying, and wide-area control.

**JAKO KILTER** (Senior Member, IEEE) received the B.Sc. and M.Sc. degrees in electrical power engineering from the Tallinn University of Technology, and the Ph.D. degree in electrical power engineering from the Tallinn University of Technology, in 2009. Currently, he is a Professor of power systems and the Head of the Power Systems Research Group, School of Engineering, Tallinn University of Technology; the Chair of the High Voltage Committee, Estonian Centre for Standardisation and Accreditation; and the Co-Chair of CIGRE Estonian National Committee. His research and consultancy work over the years has been split between the areas of power system dynamics, wide-area control and applications, and power quality.

**MARJAN POPOV** (Fellow, IEEE) received the Ph.D. degree in electrical power engineering from the Delft University of Technology, Delft, in 2002. He is a Chevening Alumnus. In 1997, he was an Academic Visitor with the University of Liverpool, Liverpool, U.K., where he was working with the Arc Research Group on modeling SF6 circuit breakers. His research interests include future power systems, large-scale power system transients, intelligent protection for future power systems, and wide-area monitoring and protection. He is a member of Cigre and actively participated in WG C4.502 and WG A2/C4.39. In 2010, he received the prestigious Dutch Hidde Nijland Prize for extraordinary research achievements. He was a recipient of the IEEE PES Prize Paper Award and the IEEE Switchgear Committee Award, in 2011. He is an Associate Editor of *International Journal of Electrical Power and Energy Systems* (Elsevier). In 2017, together with the Dutch utilities TenneT, Alliander, and Stedin, he founded the Dutch Power System Protection Centre to promote the research and education in power system protection.

**OLEG BAGLEYBTER** received the Diploma and Ph.D. degrees in electrical engineering from Irkutsk Technical University, in 1999 and 2006, respectively. He worked as a Protection and Control Engineer for one of the Russian utilities and a Product Manager of transmission protection relays at GE Grid Solutions. He is currently working as a Senior Staff Engineering Manager at GE and is responsible for Advanced Automation Applications Research and Development portfolio within the GE Grid Automation business. His focus is on developing and deploying innovative applications and solutions utilising wide area measurements in transmission and distribution grids.

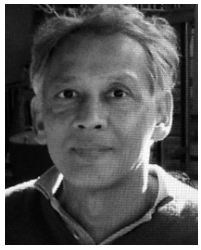

**DANNY KLAAR** received the M.Sc. degree in electric power engineering from the Delft University of Technology, in 1983. Currently, he is a System Operation Advisor at TSO TenneT. He is a member of Cigre SC C2 and participates in the JWG C2/C5.06. He is also active in the European TSO Association ENTSO-E in the field of system operations, focusing on innovative operational concepts, international collaboration among TSOs, and the impact of regulation in the view of the energy transition towards a carbon neutral society.